Int. J. Electrochem. Sci., 11 **(2016)** 3227 - 3237

International Journal of
ELECTROCHEMICAL
SCIENCE
www.electrochemsci.org

Porous $MnNi_2O_4$ Nanorods as an Efficient Bifunctional Catalyst for Rechargeable Li–O_2 battery

Jun Li[1,2†], *Yuan Li*[3†], *Kun Guo*[4], *Liangliang Zou*[1,*], *Qinghong Huang*[1], *Zhiqing Zou*[1] *and Hui Yang*[1,*]

[1] Shanghai Advanced Research Institute, Chinese Academy of Sciences (CAS), Shanghai, 201210, China
[2] University of the CAS, Beijing 100039, China
[3] Technology Center, China Tobacco Hebei Industrial Company, Ltd., Shijiazhuang 050051, China
[4] Department of Petroleum Engineering, University of Stavanger, 4036 Stavanger, Norway
†These authors contribute equally to this work
[*]E-mail: yangh@sari.ac.cn, zoull@sari.ac.cn

Received: 17 December 2015 / *Accepted:* 19 January 2016 / *Published:* 1 March 2016

Spinel-type porous $MnNi_2O_4$ nanorods are prepared using a facile electrospinning and subsequent calcination approach. A $MnNi_2O_4$ nanoparticle material is also synthesized *via* the sol-gel method to explore the effect of surface area, pore diameter and pore volume on catalytic activity. The crystal phase and morphology of the samples are confirmed by X-ray diffractometry and transmission electron microscopy. Linear sweep voltammetry analysis shows that the $MnNi_2O_4$ nanorods electrode exhibits better activities in oxygen reduction and evolution reactions than the prepared $MnNi_2O_4$ nanoparticles or Ketjenblack electrodes. The sequenced activities of these three materials are further supported by a reduction in both the discharge and recharge overpotentials during battery tests. Furthermore, batteries with the $MnNi_2O_4$ nanorods present improved rate capability and cyclability compared with the $MnNi_2O_4$ nanoparticles and Ketjenblack. This enhanced performance is explained by the large surface area, mean pore diameter, and pore volume of the $MnNi_2O_4$ nanorods. These results highlight the importance of porous $MnNi_2O_4$ nanorods as a prospective bifunctional catalyst and a potential method of electrospinning to scale up the preparation of catalysts for rechargeable Li–O_2 batteries.

Keywords: Lithium–air batteries, Bi-functional catalyst, $MnNi_2O_4$, Porous nanorods

1. INTRODUCTION

Because of their high theoretical energy capacity and low cost, lithium–air batteries have the potential to replace conventional lithium–ion batteries as the future power source of electric vehicles.[1-7] However, lithium–air batteries still suffer from slow oxygen reduction/evolution

reactions (ORR/OER) kinetics,[8] inefficient decomposition of the discharge products,[9] chemical instability of the electrolyte[10] and corrosion of the lithium anode.[11] These current challenges must be addressed before their implementation can be realized.

To improve the Li–O_2 battery performance, substantial efforts have been devoted to exploiting bifunctional catalysts which promote both the ORR/OER reactions. [12-15] MnO_2–based catalysts [16-19], which are traditional ORR catalysts, have exhibited remarkable activities in Li–O_2 batteries. For example, J. B. Goodenough's group applied a $CoMn_2O_4$–graphene composite material as a catalyst of Li–O_2 batteries and achieved a reduction of discharge and charge overpotentials.[20] The recharge voltage plateau was decreased by 500 mV and the battery was able to run for 40 cycles with a capacity limitation of 1000 mAh g_C^{-1}. Wang *et al.* also confirmed that porous $MnCo_2O_4$ spheres were effective catalysts for Li–O_2 batteries.[21] By incorporating $MnCo_2O_4$ with graphene, the Li–O_2 battery was recyclable over 50 cycles with a discharge–charge capacity of 1000 mAh g^{-1}. Chen's group prepared a $CaMnO_3$ material with an interconnected pore structure as a cathode catalyst of Li–O_2 battery.[22] They found that the voltage gap between discharge and charge of the $CaMnO_3$ electrode was 620 mV smaller than that of carbon electrode and the cyclability was also significantly improved.

Porous structure of an oxygen electrode provides a transferring channel for Li^+ and O_2 to pass through. It also affords the space for discharge products, which directly affect the discharge–charge efficiency, rate capability and cycling stability.[23] Yang *et al.* evaluated the performance of Li–O_2 batteries with different carbon cathode materials and concluded that the porosity and pore size were critical for the oxygen electrode.[24] During the discharge process, lithium oxides randomly deposit into micro-, meso- and macro- pores. When the precipitation occurs at the inlet of the micropores, the pore is blocked and mass transfer is terminated, resulting in poor utilization of pore volume. However, if the lithium oxides deposit into the meso- and the macro- pores, the diffusion of O_2 and electrolytes are not dramatically restricted. This study highlights the importance of developing an oxygen electron with optimized pore structures.

Electrospinning is an effective method to prepare nanofibers as fibrous catalysts and electrode networks. [25, 26] For example, Zhang's group synthesized perovskite–type porous $La_{0.75}Sr_{0.25}MnO_3$ nanotubes via electrospinning.[27] They found that the one–dimensional structure of this material enables rapid electron transport and O_2 intake and therefore, these materials exhibit good bifunctional activities. Batteries using their catalyst presented a 30-50 mV higher discharge plateau and a 200 mV lower recharge plateau compared to Ketjen black (KB) alone. A high discharge–charge capacity of ~10000 mAh g^{-1} was maintained at 0.025 mA cm^{-2}. More interestingly, the cyclability reached 124 cycles when restricting the discharge–charge capacity to 1000 mAh g^{-1}. Chen *et al.* utilized electrospinning to prepare porous Fe–C based catalysts, which also exhibit better ORR activity, recyclability and lower cost compared to commercial Pt-based catalysts. [28]

Although various spinel-type oxides have been reported with remarkable performance as catalysts of Li–O_2 batteries. Little interest, however, is ever shown to the $MnNi_2O_4$, which is another attractive spinel-type oxide due to the combination of prevailing Mn and Ni elements, low cost and toxicity. In this work, sol–gel and electrospinning methods are employed to prepare $MnNi_2O_4$ nanoparticles (NPs) and porous nanorods (NRs). The influence of the specific area, pore structure and morphology of the materials on their performance in Li–O_2 batteries is investigated. The goal of this

work is to enhance the performance of Li–air batteries by producing a highly active catalyst and reducing the discharge/charge overpotentials.

2. EXPERIMENTS

2.1. Preparation of $MnNi_2O_4$

2.1.1. Synthesis of $MnNi_2O_4$ NPs

Sol–gel method is used to prepare $MnNi_2O_4$ NPs. A solution containing citric acid, nickel nitrate and manganese nitrate with the molar ratio of 4 :2 :1 is adjusted with ammonia to obtain a pH value of 8. The solution is then stirred at 40 °C to form a gel. Afterwards, this gel is heated to 350 °C for 2 hours to ensure the complete decomposition of organic solvent and further calcined at 800 °C for 5 hours to gain the final products.

2.1.2. Synthesis of porous $MnNi_2O_4$ NRs

Nickel nitrate and manganese nitrate precursors with a molar ratio of 2 : 1 are dissolved in deionized water with 10 times of the mass of the salts. Poly(vinylpyrrolidone) (PVP) is then added to reach 15 wt % and dissolved with stirring. The injection speed of electrospinning is maintained at 0.06 mL h^{-1}. The distance between pinhead and receptor is 15 cm and the voltage is 16~18 kV. After electrospinning, the sample is heated at 350 °C for 2h in a muffle under air atmosphere to ensure the complete decomposition of organic solvent and further calcined at 800 °C for 5 hours.

2.2. Physical characterization

The crystal phase and purity of the products were characterized by X–ray powder diffraction (XRD), recorded on a Bruker–AXS micro-diffractometer (D8 ADVANCE) using Cu Kα radiation. The morphology and structure of the catalysts and cathodes were obtained from field emission scanning electron microscopy (FESEM, HITACHI S–4800) and high–resolution transmission electron microscopy (HRTEM, JEOL JEM–2100F). Nitrogen adsorption–desorption measurements were performed at 77 K on a Micromeritics ASAP 2020 adsorption analyzer, and the specific surface area was calculated via the Brunauer–Emmett–Teller (BET) method.

2.3. Electrochemical characterization

Typically, the oxygen cathode was prepared by painting homogenous ink slurry onto C–paper current collector with a loading of 2.0 ± 0.2 mg cm^{-2}. The ultrasonicated ink slurry was composed of a mixture of 45 wt. % catalysts, 45 wt. % KB carbon and 10 wt. % polytetrafluoroethylene (PTFE) binder, dispersed in isopropanol and water (volume ratio of 1:1) [29-32]. Subsequently, the oxygen

electrodes were vacuum–dried at 80 °C for at least 12 h prior to being transferred into an Ar–filled glovebox ([H_2O] < 0.1 ppm, [O_2] < 0.1 ppm). Swagelok-type Li–O_2 batteries were assembled inside a glove box using a lithium foil (16 mm diameter) as anode, a glass–fiber and a polypropylene (Celgard 2400) as separator, and 1 M $LiCF_3SO_3$–TEGDME as electrolyte. After assembly, the batteries were placed into an oxygen–filled glass bottle with the gas pressure maintained at 1 atm. The galvanostatic discharge–charge tests were proceeded within a voltage window of 2.0–4.4 V_{Li} on a LAND battery testing system. Linear scanning voltammetry (LSV) was conducted in a three–electrode electrochemical cell with a CHI 730B electrochemical workstation. Aforesaid oxygen electrode was used as the working electrode, lithium metal foils were used as the counter electrode and reference electrode, respectively. In all tests, the scan rate of 10 mV s^{-1}. Prior to each experiment, the electrolyte solutions were purged with N_2 to calibrate the background current or O_2 as a reactant for at least 30 minutes.

3. RESULTS AND DISCUSSION

Fig. 1a and 1b show the XRD patterns of the prepared $MnNi_2O_4$ NPs and porous $MnNi_2O_4$ NRs, respectively. Both match the X-Ray diffraction of spinel $MnNi_2O_4$ (JCPDS No. 36–0083), which is shown in Fig. 1c. The diffraction peaks at 18.43°, 30.24°, 35.43°, 37.37°, 57.13°and 62.73° correspond to the crystal plane of (111), (220), (311), (222), (511) and (440), respectively. In addition, there is no other obvious diffraction peak, indicating that both materials have good purity.

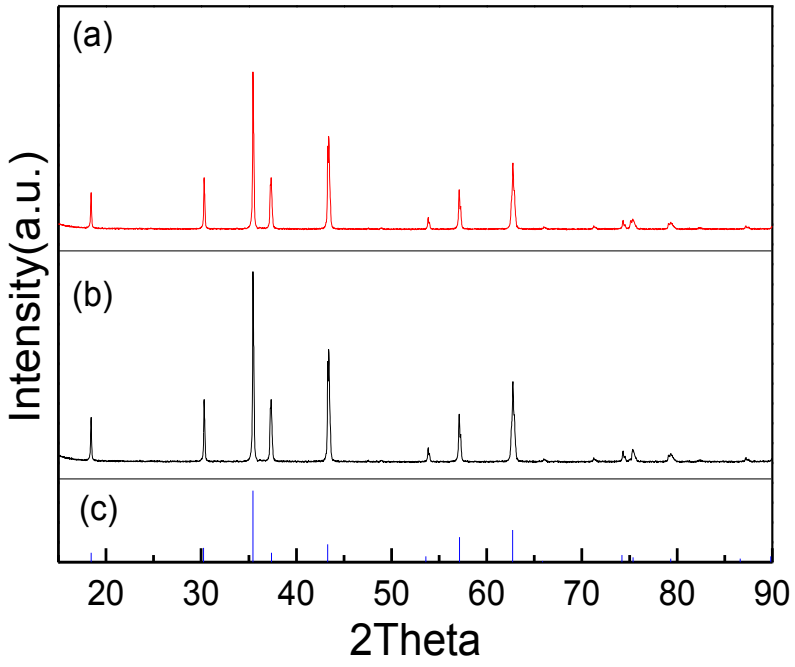

Figure 1. XRD patterns of $MnNi_2O_4$ NPs (a), porous $MnNi_2O_4$ NRs (b) and standard JCPDS 36–0083 (c).

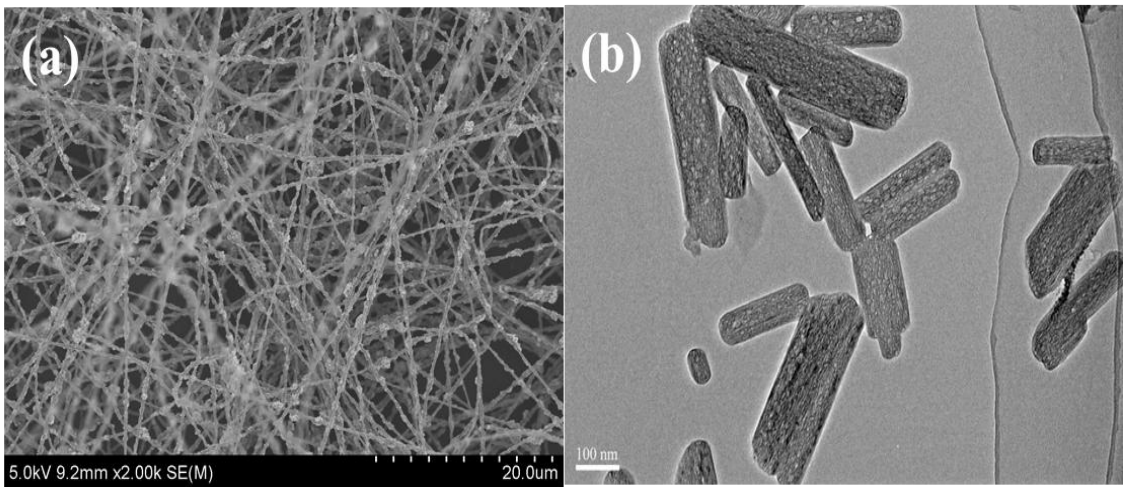

Figure 2. FESEM (a) image of the $MnNi_2O_4$ NRs sample before calcination and TEM (b) image of the sample after calcination.

Fig. 2a illustrates the morphology of the $MnNi_2O_4$ sample before calcination. At this stage, nanofibers cover the surface along with unevenly distributed particles. These particles may be a result from the segregation of precursors in the solution. Fig. 2b shows the TEM image of the $MnNi_2O_4$ sample after calcination. The nanofibers shown before calcination were decomposed into separate porous NRs with lengths from 100 to 500 nm. The gas products produced in the process of PVP combustion may account for the generation of these pores and channels. Table 1 compares the BET surface area, mean pore diameter and pore volume of the two $MnNi_2O_4$ samples. Porous $MnNi_2O_4$ NRs have much larger surface area and pore volume, and a slightly bigger mean pore diameter than that of the $MnNi_2O_4$ NPs.

Table 1. BET specific area and pore structural properties of $MnNi_2O_4$ NPs and NRs.

Sample	specific area /$m^2\ g^{-1}$	Mean pore diameter/nm	Pore volume/$cm^3\ g^{-1}$
$MnNi_2O_4$ NPs	5.1	31.3	0.023
$MnNi_2O_4$ NRs	31.5	33.4	0.079

The OER and the ORR activities of the two samples were analyzed using the LSV technique. Fig. 3a depicts the ORR curves for the $MnNi_2O_4$ NP-, the $MnNi_2O_4$ NR- and the KB- electrodes conducted in 1 M $LiCF_3SO_3$–TEGDME. The onset potential of each sample is slightly higher than that of the theoretical value (2.96 V_{Li}). This variation may be due to contribution from Li^+ intercalations into KB, the presence of $MnNi_2O_4$ oxides, capacitive behavior, or the presence of side reactions such as electrolyte decomposition and carbon corrosion. [33-35] In any case, both the ORR onset potentials and current densities follow the order of $MnNi_2O_4$ NRs > $MnNi_2O_4$ NPs > KB, demonstrating that $MnNi_2O_4$ NRs exhibit the best catalytic activity among these materials. Similarly, an LSV analysis of the OER activity was operated in a nitrogen-saturated 1 M $LiCF_3SO_3$–TEGDME solution (Fig. 3b).

Compared with the KB electrode, the $MnNi_2O_4$ NP electrode exhibits a lower OER onset potential and a larger current density, indicating better OER activity. What's more, the $MnNi_2O_4$ NR electrode shows the lowest onset potential and largest current density. This improved performance can be ascribed to the material having a higher surface area, larger pore diameters and pore volumes. This allows for more active sites to facilitate the transportation of electrons and O_2. Therefore, the prepared $MnNi_2O_4$ NRs are a potential bifunctional catalyst for use in Li–O_2 battery.

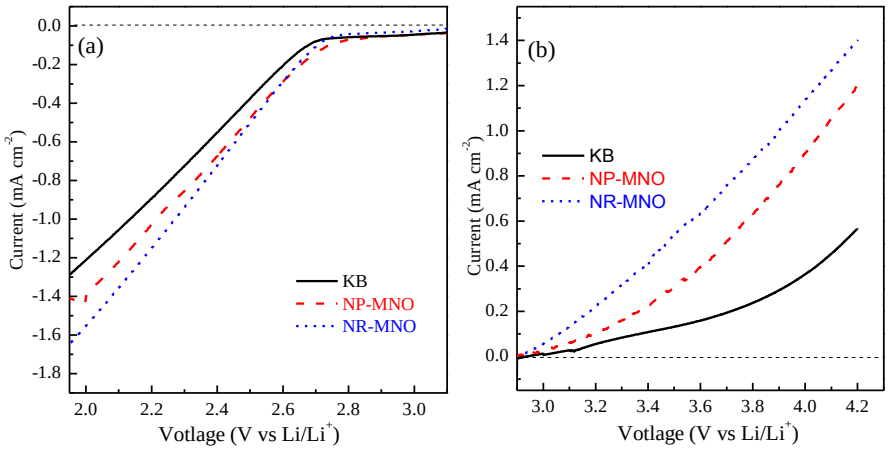

Figure 3. LSV curves of the ORR (a) and OER (b) on $MnNi_2O_4$ NRs、$MnNi_2O_4$ NPs and KB electrodes in 1 M $LiCF_3SO_3$ in TEGDME at a scan rate of 10 mV s^{-1}.

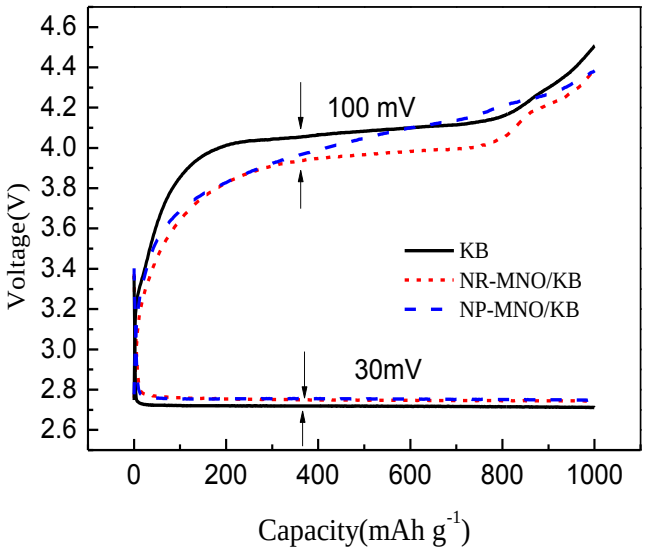

Figure 4. The first discharge–charge curves of Li–O_2 batteries with $MnNi_2O_4$ NP/KB, $MnNi_2O_4$ NR/KB and KB with a capacity restriction of 1000 mAh g^{-1} at 0.1 mA cm^{-2}.

After evaluating the activity of the catalysts, their performance was tested in battery models. Fig. 4 illustrates the discharge and recharge curves of the batteries with $MnNi_2O_4$ NR-, $MnNi_2O_4$ NP-

and KB- electrodes with a capacity limitation of 1000 mAh g^{-1} at 0.1 mA cm^{-2}. The $MnNi_2O_4$ NR- and $MnNi_2O_4$ NP- electrodes show nearly the same discharge plateau which is 30 mV higher than the discharge plateau of the KB electrode. This suggests that the prepared materials have a reduced ORR polarization. Furthermore, the $MnNi_2O_4$ NR electrode has a recharge voltage plateau that is 100 mV less than that of the KB electrode and also has a high round–trip efficiency of 71.0 %. These results show that the $MnNi_2O_4$ NRs effectively reduce the discharge–charge polarizations and enhance the energy efficiency compared to the KB standard.

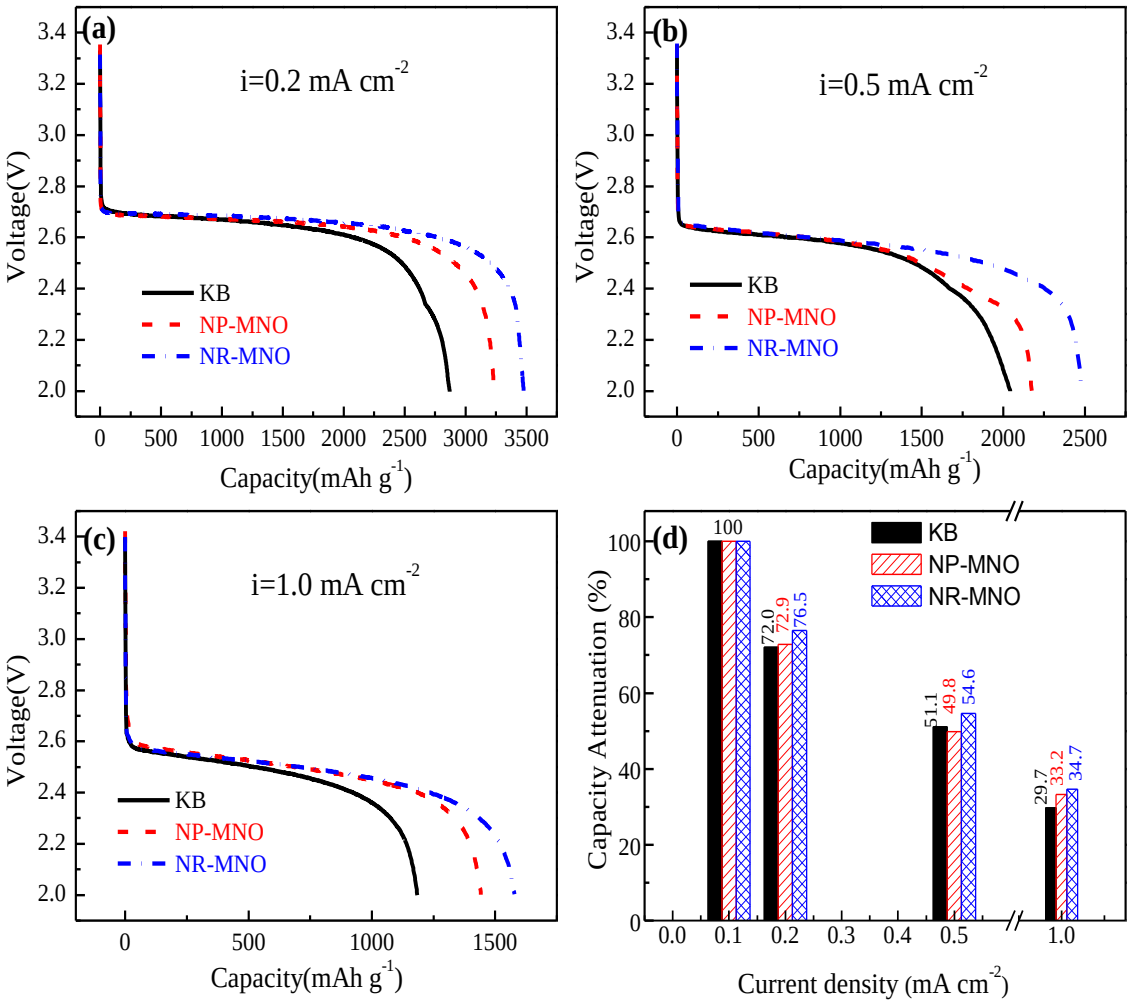

Figure 5. Discharge curves of the Li–O_2 batteries with $MnNi_2O_4$ NR/KB, $MnNi_2O_4$ NP/KB and KB as catalysts at 0.2 (a), 0.5 (b), and 1.0 (c) mA cm^{-2}. Retention rate of each sample compared to the capacity at 0.1 mA cm^{-2} (d).

Rate capability is an important characteristic for secondary batteries. The discharge curves of the batteries with $MnNi_2O_4$NR-, $MnNi_2O_4$NP- and KB- electrodes at different current densities are shown in Fig. 5. At higher densities, the discharge plateaus of the batteries with $MnNi_2O_4$ NR and $MnNi_2O_4$ NP electrodes were relatively higher than for the battery with a KB electrode. For each sample, the discharge capacity and discharge voltage decreased at the current density increased. The

capacity retention data in Fig. 5d further demonstrates that the incorporation of $MnNi_2O_4$ NRs helps the Li–O_2 batteries to exhibit enhanced rate capability.

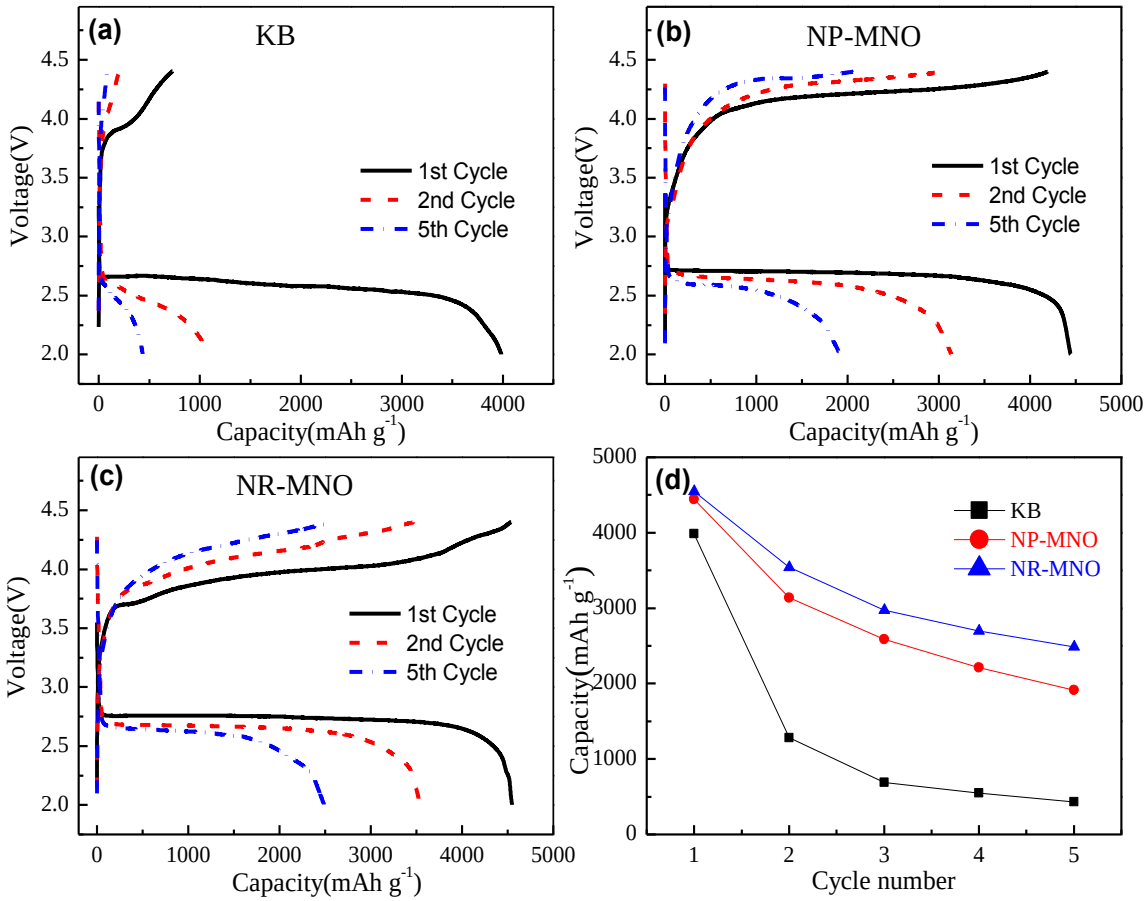

Figure 6. Discharge-charge curves (a, b and c) and cycling performance comparison (d) for the first 5 cycles of Li–O_2 batteries with KB (a), $MnNi_2O_4$ NP/KB (b) and $MnNi_2O_4$ NR/KB (c) in the voltage range of 2.0-4.4 V_{Li} at 0.1 mA cm^{-2}.

Fig. 6 illustrates the discharge-charge curves for the first 5 cycles of the batteries with $MnNi_2O_4$ NR-, $MnNi_2O_4$ NP- and KB- electrodes at 0.1 mA cm^{-2} over a voltage range of 2.0-4.4 V_{Li}. The performance of the KB electrode gradually degrades giving a low capacity retention of 10.7%. This is due to an insufficient decomposition of discharge products that cover the electrode surface which inhibits O_2 intake as well as Li^+ and electron transport. [30, 36] On the contrary, batteries with $MnNi_2O_4$ NRs and $MnNi_2O_4$ NPs electrodes achieve specific capacities of 2488 and 1917 mAh g^{-1} with capacity retention ratios of 54.7 % and 43.1 %, respectively. It should also be noted that the batteries with the prepared electrodes still decay continuously which is reasonably attributed to the considerable accumulation of Li_2O_2, carbon corrosion, and the formation of undesirable by-products that cannot be recovered during cycling. [29, 31, 33]

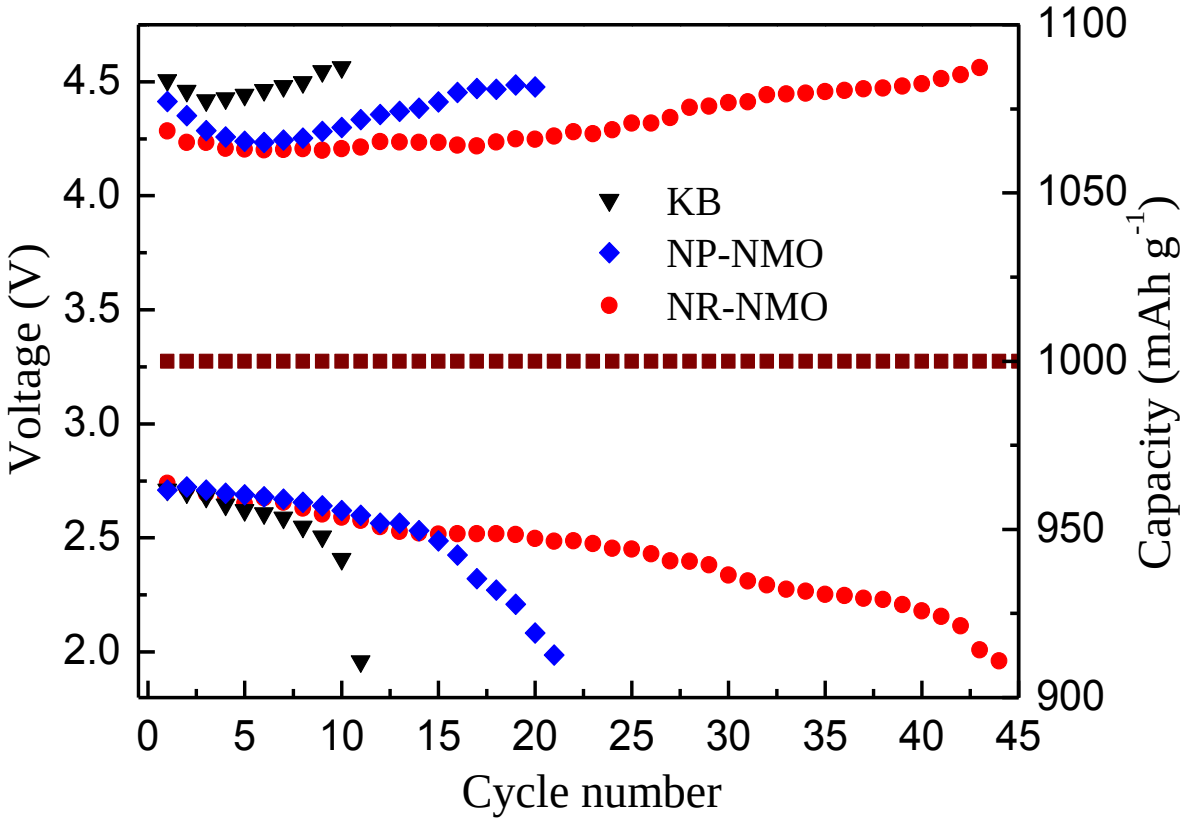

Figure 7. The terminal voltage profiles of the Li–O_2 batteries with bare KB, $MnNi_2O_4$ NP/KB and$MnNi_2O_4$ NR/KB with a capacity restriction of 1000 mAh g^{-1} at 0.1 mA cm^{-2}.

By limiting the discharge-charge depth, the cyclability of the battery can be greatly extended. Fig. 7 shows the terminal voltage data of batteries with $MnNi_2O_4$ NR-, $MnNi_2O_4$ NP- and KB-electrodes at a capacity limitation of 1000 mAh g^{-1}. In this case, batteries with $MnNi_2O_4$ NR-, $MnNi_2O_4$ NP- and KB- electrodes can run 10, 21 and 44 cycles, respectively, until the terminal voltages fall below 2.0 V_{Li}. This improved cyclability highlights the superior ORR and OER activities of the $MnNi_2O_4$ NR electrode. In addition, the recharge terminal voltages the of the $MnNi_2O_4$ NR electrode for the first 30 cycles were below 4.5 V_{Li}. This proves that $MnNi_2O_4$ NR electrode has a better recharge efficiency than that of KB electrode. These could be attributed to the porous structures of $MnNi_2O_4$ NR that ensuring not only provide many electrocatalytic sites and pore volume for nucleation or accommodation of Li_2O_2 discharge products, but also promote the flow of gases and infiltration of the electrolyte, and eventually improve the cyclability. [32, 37]

4. CONCLUSIONS

In summary, Sol-gel and electrospinning methods were used to prepare $MnNi_2O_4$ samples with different morphologies and pore structures, *i.e.* $MnNi_2O_4$ NR and porous $MnNi_2O_4$ NP, respectively, which were evaluated as catalysts for rechargeable Li–O_2 batteries. Compared with the carbon only

electrode, the $MnNi_2O_4$ materials exhibit enhanced charge/discharge efficiency, rate capability and cycling performance. Especially, the Li-O_2 batteries employing mesoporous $MnNi_2O_4$ NR materials as cathode catalysts achieve a high specific capacity of 4547mAh g^{-1}, and enhance cyclability with a 100 mV smaller discharge-recharge voltage gap than that of the carbon-only cathode at a current rate of 100mA g^{-1}.The prepared porous $MnNi_2O_4$ NR material together with the readily available electrospinning method can be useful for future development of reversible Li–O_2 batteries.

ACKNOWLEDGEMENTS
We would like to thank the National Basic Research Program of China (973 Program) (No. 2012CB932800), the National High-tech R&D Program of China (863Program) (No. 2015AA060603); and the Drexel–SARI Global Funding Scheme for support of this work.

References

1. J. Christensen, P. Albertus, R.S. Sanchez-Carrera, T. Lohmann, B. Kozinsky, R. Liedtke, J. Ahmed, A. Kojic, *J Electrochem Soc*, 159 (2012) R1.
2. Z.M. Cui, L.J. Li, A. Manthiram, J.B. Goodenough, *J Am Chem Soc*, 137 (2015) 7278.
3. L. Hui, W. Chuan, W. Feng, B. Ying, *Rare Metal Mat Eng*, 43 (2014) 1525.
4. A.C. Luntz, B.D. McCloskey, *Chem Rev*, 114 (2014) 11721.
5. T.H. Yoon, Y.J. Park, *Rsc Adv*, 4 (2014) 17434.
6. J.L. Yuan, J.S. Yu, B. Sunden, *J Power Sources*, 278 (2015) 352.
7. N. Zhao, C.L. Li, X.X. Guo, *Energy Technol-Ger*, 2 (2014) 317.
8. A. Kumar, F. Ciucci, A.N. Morozovska, S.V. Kalinin, S. Jesse, *Nat Chem*, 3 (2011) 707.
9. T. Zhang, H. Zhou, *Nat Commun*, 4 (2013) 1817.
10. V.S. Bryantsev, V. Giordani, W. Walker, M. Blanco, S. Zecevic, K. Sasaki, J. Uddin, D. Addison, G.V. Chase, *J Phys Chem A*, 115 (2011) 12399.
11. G. Girishkumar, B. McCloskey, A.C. Luntz, S. Swanson, W. Wilcke, *J Phys Chem Lett*, 1 (2010) 2193.
12. J.G. Kim, Y. Kim, Y. Noh, W.B. Kim, *Chemsuschem*, 8 (2015) 1752.
13. A. Nacy, X. Ma, E. Nikolla, *Topics in Catalysis*, 58 (2015) 513.
14. W. Yang, J. Salim, S. Li, C. Sun, L. Chen, J.B. Goodenough, Y. Kim, *J Mater Chem*, 22 (2012) 18902.
15. H.W. Park, D.U. Lee, M.G. Park, R. Ahmed, M.H. Seo, L.F. Nazar, Z. Chen, *Chemsuschem*, 8 (2015) 1058.
16. T. Zhang, F. Cheng, J. Du, Y. Hu, J. Chen, *Adv Energy Mater*, 5 (2015) n/a.
17. K. Selvakumar, S.M. Senthil Kumar, R. Thangamuthu, G. Kruthika, P. Murugan, *Int J Hydrogen Energy*, 39 (2014) 21024.
18. H. Geaney, C. O'Dwyer, *Phys Chem Chem Phys*, 17 (2015) 6748.
19. J. Zhang, Y. Luan, Z. Lyu, L. Wang, L. Xu, K. Yuan, F. Pan, M. Lai, Z. Liu, W. Chen, *Nanoscale*, 7 (2015) 14881.
20. L. Wang, X. Zhao, Y.H. Lu, M.W. Xu, D.W. Zhang, R.S. Ruoff, K.J. Stevenson, J.B. Goodenough, *J Electrochem Soc*, 158 (2011) A1379.
21. S. Ma, L. Sun, L. Cong, X. Gao, C. Yao, X. Guo, L. Tai, P. Mei, Y. Zeng, H. Xie, R. Wang, *J Phys Chem C*, 117 (2013) 25890.
22. X. Han, Y. Hu, J. Yang, F. Cheng, J. Chen, *Chem Commun*, 50 (2014) 1497.
23. H.C. Lee, V. Roev, T.Y. Kim, M.-S. Park, D. Im, *Meeting Abstracts*, MA2015-01 (2015) 427.
24. C. Tran, X.Q. Yang, D.Y. Qu, *J Power Sources*, 195 (2010) 2057.

25. P. Chen, H. Wu, T. Yuan, Z. Zou, H. Zhang, J. Zheng, H. Yang, *J Power Sources,* 255 (2014) 70.
26. N. Bhardwaj, S.C. Kundu, *Biotechnol Adv,* 28 (2010) 325.
27. J. Xu, D. Xu, Z. Wang, H. Wang, L. Zhang, X. Zhang, *Angew Chem Int Edit,* 52 (2013) 3887.
28. J. Wu, H.W. Park, A. Yu, D. Higgins, Z. Chen, *J Phys Chem C,* 116 (2012) 9427.
29. Y. Li, K. Guo, J. Li, X. Dong, T. Yuan, X. Li, H. Yang, *ACS Appl Mater Interfaces,* 6 (2014) 20949.
30. K. Guo, Y. Li, T. Yuan, X. Dong, X. Li, H. Yang, *J Solid State Electr,* (2014).
31. K. Guo, Y. Li, J. Yang, Z. Zou, X. Xue, X. Li, H. Yang, *J. Mater. Chem. A,* 2 (2014) 1509.
32. H. Wang, Y. Yang, Y. Liang, G. Zheng, Y. Li, Y. Cui, H. Dai, *Energ Environ Sci,* 5 (2012) 7931.
33. B.D. Adams, C. Radtke, R. Black, M.L. Trudeau, K. Zaghib, L.F. Nazar, *Energ Environ Sci,* 6 (2013) 1772.
34. J.R. Harding, Y.C. Lu, Y. Tsukada, Y. Shao-Horn, *Phys Chem Chem Phys,* 14 (2012) 10540.
35. A. Kraytsberg, Y. Ein-Eli, *J Power Sources,* 196 (2011) 886.
36. J. Read, *J Electrochem Soc,* 149 (2002) A1190.
37. P. Li, W. Sun, Q. Yu, M. Guan, J. Qiao, Z. Wang, D. Rooney, K. Sun, *Materials Letters,* 158 (2015) 84.